Electronic Supplementary Information

Functional Microscale Single-phase White Emission Lanthanide MOF for Tunable Fluorescent Sensing and Water Quality Monitoring

Tiancheng Sun, Ping Wang, Ruiqing Fan, Wei Chen, Sue Hao and Yulin Yang**

T. Sun, P. Wang, Prof. R. Fan, W. Chen, S. Hao and Prof. Y. Yang
MIIT Key Laboratory of Critical Materials Technology for New Energy Conversion and Storage, School of Chemistry and Chemical Engineering, Harbin Institute of Technology, Harbin 150001, P. R. China

Contents

Section 1. Experimental Section

Materials and Methods

All chemicals for the syntheses were commercially available reagents of analytical grade and were used without further purification. IR spectra were obtained from KBr pellets using a Nicolet Avatar-360 infrared spectrometer in the 4000–400 cm^{-1} region. Elemental analyses were performed on a PerkinElmer 240c element analyzer. Concentrations of Eu, Tb and Gd were determined by using a ThermoScientific XSERIES 2 inductively coupled plasma-mass spectrome-try (ICP-MS) system. The thermal analyses were performed on a ZRY-2P thermogravimetric analyzer from 30 °C to 700 °C with a heating rate of 10 °C min^{-1} under air. UV-vis spectra were obtained on a Perkin-Elmer Lambda 20 spectrometer. Scan electron microscope (SEM) images were recorded by Rili SU 8000HSD Series Hitachi New Generation Cold Field Emission SEM. XPS experiments were carried out on a RBD upgraded PHI-5000C ESCA system (Perkin Elmer) with Mg Kα radiation (hv = 1253.6 eV). Powder X-ray diffraction (PXRD) patterns were recorded in the 2θ range of 5°–50° using Cu-Kα radiation with a Shimadzu XRD-6000 X-ray diffractometer. The simulation of PXRD pattern was carried out using the single-crystal data and diffraction-crystal module of the Mercury (Hg) program version 3.0. All the fluorescence measurements were recorded on an Edinburgh FLS 920 fluorescence spectrometer in the range of 380–750 nm. The quantum yields (QY) of solid samples were measured in the same instrument using the absolute method with a G8 integration sphere (GMP SA, Switzerland) covered by Spectralone in the same

instrument. All QY measurements were performed in triplicate and averaged. Time-resolved fluorescence decay curves of coordination polymers are well fitted into a mono-exponential function: $I_0 = I + A \exp(-t/\tau)$, where I and I_0 are the luminescent intensities at time $t = t$ and $t = 0$, whereas τ is defined as the luminescent lifetime, and a biexponential function: $I = I_0 + A_1 \exp(-t/\tau_1) + A_2 \exp(-t/\tau_2)$, where I and I_0 are the luminescent intensities at time $t = t$ and $t = 0$, respectively, whereas τ_1 and τ_2 are defined as the luminescent lifetimes, the average lifetime $<\tau>$ was calculated according to the following equation: $<\tau> = \frac{\tau_1^2 A_1\% + \tau_2^2 A_2\%}{\tau_1 A_1\% + \tau_2 A_2\%}$.

Syntheses of {[Nd(DPON)(H_2O)$_2$]·(H_2O)}$_n$ (1-Nd)

A mixture of $Nd(NO_3)_3 \cdot 6H_2O$ (0.05 mmol, 21.9 mg), H_3DPON (0.1 mmol, 30.3 mg) and 6 mL of the mixed solvent of deionized water and DMF (4:2) was placed in a Teflon reactor (20 mL). After stirred for 30 min in air, the pH of the reaction mixture was adjusted to 4.0 by HNO_3, then heated at 120 °C for 3 h. The mixture was gradually cooled to room temperature at a rate of 5 °C h^{-1}, purple flake crystals of **1-Nd** were collected and washed with distilled water and then dried under atmosphere (yield 93% based on Nd (III)). Anal. Calcd for $C_{14}H_{12}NdNO_{10}$ (%): C, 33.73%; H, 2.43%; N, 2.81%. Found: C, 33.71%; H, 2.43%; N, 2.82%. IR (KBr pellet, cm^{-1}): 3461 (w), 1538 (vs), 1384 (vs), 1300 (s), 1260 (s), 1240 (s), 1209 (s), 1155 (m), 1104 (w), 1060 (w), 1023 (m), 969 (w), 893 (vw), 849 (w), 788 (s), 672 (w), 631 (w), 556 (vw), 502 (vw), 477 (vw), 424 (m), 416 (m), 406 (m).

Syntheses of {[Sm(DPON)(H_2O)$_2$]·(H_2O)}$_n$ (2-Sm)

The procedure for coordination polymer **2-Sm** was similar to that of coordination

polymer **1-Nd** except $Sm(NO_3)_3 \cdot 6H_2O$ (0.05 mmol, 22.2 mg) was used instead of $Nd(NO_3)_3 \cdot 6H_2O$. Colorless flake crystals of **2-Sm** were collected and washed with distilled water and then dried under atmosphere (yield 95% based on Sm(III)). Anal. Calcd for $C_{14}H_{12}SmNO_{10}$ (%): C, 33.32%; H, 2.40%; N, 2.78%. Found: C, 33.33%; H, 2.40%; N, 2.76%. IR (KBr pellet, cm^{-1}): 3489 (w), 1541 (vs), 1383 (vs), 1301 (s), 1262 (s), 1241 (s), 1211 (s), 1155 (m), 1114 (vw), 1079 (vw), 1025 (m), 971 (w), 931 (vw), 900 (vw), 884 (w), 851 (m), 836 (s), 812 (s), 788 (s), 687 (m), 672 (m), 631 (m), 558 (w), 478 (w), 453 (m), 434 (m), 422 (s), 404 (s).

Syntheses of $\{[Eu(DPON)(H_2O)_2]\cdot(H_2O)\}_n$ (3-Eu)

The procedure for coordination polymer **3-Eu** was similar to that of coordination polymer **1-Nd** except $Eu(NO_3)_3 \cdot 6H_2O$ (0.05 mmol, 22.3 mg) was used instead of $Nd(NO_3)_3 \cdot 6H_2O$. Colorless flake crystals of **3-Eu** were collected and washed with distilled water and then dried under atmosphere (yield 93% based on Eu(III)). Anal. Calcd for $C_{14}H_{12}EuNO_{10}$ (%): C, 33.22%; H, 2.39%; N, 2.77%. Found: C, 33.25%; H, 2.39%; N, 2.76%. IR (KBr pellet, cm^{-1}): 3484 (w), 1541 (vs), 1379 (vs), 1300 (vs), 1261 (s), 1240 (s), 1211 (s), 1155 (m), 1138 (m), 1116 (w), 1079 (vw), 1025 (m), 972 (w), 931 (vw), 883 (w), 851 (m), 835 (m), 812 (m), 787 (s), 687 (w), 672 (w), 631 (m), 602 (w), 577 (w), 557 (w), 470 (w), 454 (w), 440 (w), 423 (m), 410 (m), 404 (w).

Syntheses of $\{[Gd(DPON)(H_2O)_2]\cdot(H_2O)\}_n$ (4-Gd)

The procedure for coordination polymer **4-Gd** was similar to that of coordination polymer **1-Nd** except $Gd(NO_3)_3 \cdot 6H_2O$ (0.05 mmol, 22.6 mg) was used instead of $Nd(NO_3)_3 \cdot 6H_2O$. Colorless flake crystals of **4-Gd** were collected and washed with

distilled water and then dried under atmosphere (yield 96% based on Gd(III)). Anal. Calcd for $C_{14}H_{12}GdNO_{10}$ (%): C, 32.87%; H, 2.36%; N, 2.74%. Found: C, 32.85%; H, 2.36%; N, 2.75%. IR (KBr pellet, cm^{-1}): 3488 (w), 1537 (vs), 1383 (vs), 1300 (vs), 1262 (s), 1240 (s), 1215 (s), 1155 (m), 1137 (m), 1115 (w), 1080 (w), 1024 (m), 973 (w), 932 (vw), 901 (vw), 884 (w), 862 (m), 854 (m), 836 (s), 812 (s), 787 (s), 688 (m), 673 (m), 654 (w), 631 (m), 602 (w), 578 (w), 558 (w), 538 (w), 478 (w), 458 (m), 443 (m), 428 (m), 415 (s).

Syntheses of $\{[Tb(DPON)(H_2O)_2]\cdot(H_2O)\}_n$ (5-Tb)

The procedure for coordination polymer **5-Tb** was similar to that of coordination polymer **1-Nd** except $Tb(NO_3)_3\cdot6H_2O$ (0.05 mmol, 22.7 mg) was used instead of $Nd(NO_3)_3\cdot6H_2O$. Colorless flake crystals of **5-Tb** were collected and washed with distilled water and then dried under atmosphere (yield 94% based on Tb(III)). Anal. Calcd for $C_{14}H_{12}TbNO_{10}$ (%): C, 32.77%; H, 2.36%; N, 2.73%. Found: C, 32.78%; H, 2.36%; N, 2.74%. IR (KBr pellet, cm^{-1}): 3491 (w), 1541 (vs), 1386 (vs), 1300 (s), 1262 (s), 1241 (s), 1210 (m), 1156 (m), 1138 (m), 1115 (w), 1080 (w), 1026 (m), 972 (w), 932 (w), 902 (vw), 884 (w), 863 (m), 854 (m), 836 (s), 813 (s), 788 (s), 687 (m), 673 (m), 654 (w), 632 (m), 604 (w), 577 (w), 560 (w), 540 (vw), 481 (w), 456 (m), 429 (m), 420 (m), 416 (m), 406 (m).

Syntheses of $\{[Dy(DPON)(H_2O)_2]\cdot(H_2O)\}_n$ (6-Dy)

The procedure for coordination polymer **6-Dy** was similar to that of coordination polymer **1-Nd** except $Dy(NO_3)_3\cdot6H_2O$ (0.05 mmol, 22.9 mg) was used instead of $Nd(NO_3)_3\cdot6H_2O$. Colorless flake crystals of **6-Dy** were collected and washed with

distilled water and then dried under atmosphere (yield 95% based on Dy(III)). Anal. Calcd for $C_{14}H_{12}DyNO_{10}$ (%): C, 32.54%; H, 2.34%; N, 2.71%. Found: C, 32.56%; H, 2.34%; N, 2.70%. IR (KBr pellet, cm^{-1}): 3487 (w), 1542 (vs), 1454 (m), 1383 (vs), 1300 (s), 1261 (s), 1240 (s), 1211 (s), 1156 (m), 1138 (m), 1115 (w), 1080 (w), 1024 (s), 972 (m), 933 (vw), 884 (w), 854 (m), 836 (s), 813 (s), 788 (s), 687 (m), 673 (m), 631 (m), 601 (w), 578 (w), 559 (w), 477 (w), 423 (s), 416 (m), 405 (m).

Syntheses of $\{[Eu_{0.059}Tb_{0.051}Gd_{0.89}(DPON)(H_2O)_2]\cdot(H_2O)\}_n$

The doping coordination polymer was also similar to that of coordination polymer **1-Nd** except using 0.059: 0.051 :0.89 ratios of $Eu(NO_3)_3\cdot6H_2O$, $Tb(NO_3)_3\cdot6H_2O$ and $Gd(NO_3)_3\cdot6H_2O$ instead of $Nd(NO_3)_3\cdot6H_2O$. The reaction time is reduced to 1h to obtain microcrystals. Colorless microcrystals of **$Eu_{0.059}Tb_{0.051}Gd_{0.89}$-DPON** were collected and washed with distilled water and then dried under atmosphere (yield 95% based on Ln(III)). Anal. Calcd (%): C, 32.89%; H, 2.37%; N, 2.74%. Found: C, 32.91%; H, 2.37%; N, 2.73%. IR (KBr pellet, cm^{-1}): 3487 (w), 1543 (vs), 1454 (m), 1383 (vs), 1300 (s), 1261 (s), 1240 (s), 1211 (s), 1156 (m), 1138 (m), 1115 (w), 1080 (w), 1024 (s), 971 (m), 933 (vw), 884 (w), 854 (m), 836 (s), 813 (s), 788 (s), 687 (m), 673 (m), 631 (m), 601 (w), 578 (w), 560 (w), 478 (w), 423 (s), 415 (m), 405 (m).

White Light Adjustment

We have synthesized a series of heterometallic Ln-MOFs $Eu_xTb_yGd_{1-x-y}$-DPON with different ratios of Eu/Tb/Gd to introduce multiple fluorescent centers. With the decrease of Eu/Tb ratio, the characteristic emission peaks of Tb^{3+} gradually increased,

while those of Eu^{3+} decrease under 321 nm excitation (Fig. 2a). CIE coordinates gradually change from red to yellow, and finally close to the green area (Fig. 2b). Then **$Eu_{0.059}Tb_{0.051}Gd_{0.89}$-DPON** is selected to balance the intensity of red and green light and its photophysical properties under different excitation wavelength are investigated (Fig. 2c). Under low-wavelength excitation, it exhibited apparent characteristic emission of Eu^{3+} and Tb^{3+}. Emission intensity of Ln^{3+} gradually increased with excitation wavelength and reached a maximum at 321 nm excitation. As the excitation wavelength increase to 325 nm, the broad emission of the ligand gradually appeared at blue light region. Upon increase to 340 nm, the emission intensities of ligand, Eu^{3+} and Tb^{3+} are comparable, which result in white light emission. Therefore, a single-phase white light MOF was obtained with CIE coordinates of (0.333, 0.335) under 340 nm excitation. The fluorescence lifetime values are τ_{Tb} = 0.801 ms and τ_{Eu} = 0.362 ms, and the overall quantum yield is about 15.2% (Table S9 and S11). In addition, $Eu_{0.059}Tb_{0.051}Gd_{0.89}$-DPON exhibit almost the same Ln^{3+} fluorescence lifetime as 3-Eu and 5-Tb (Table S11), thus the energy transfer from Tb^{3+} to Eu^{3+} in $Eu_{0.059}Tb_{0.051}Gd_{0.89}$-DPON hardly exists.

Detection for Formol in Vapor

In order to facilitate the operation when used as fluorescent probe, $Eu_{0.059}Tb_{0.051}Gd_{0.89}$-DPON was doped into polyvinyl alcohol (PVA) to form a thin film and the obtained fluorescence film show a similar emission performance compared to $Eu_{0.059}Tb_{0.051}Gd_{0.89}$-DPON powder, except a reduction in emission intensity (Fig. S17). The compartment with a hole in the container is to ensure that the

concentration of formol increases slowly and steadily. Taking the precise determination of formol concentration into account, an air formol detector is set next to the $Eu_{0.059}Tb_{0.051}Gd_{0.89}$-DPON PVA film in the device (Fig. 6c). 10 μL formol with different concentrations were respectively added into the container (16 L) to provide the formol atmosphere and closed the lid, then waited for formol to evaporate and diffuse in closed container. When the formol detector showed a stable concentration, the film was taken out and recorded for emission spectra under 340 nm excitation. The emission spectra response to the formol in vapor are recorded in Fig. S18. Comparing the fluorescence intensity at 544 nm, a sudden drop occurs at the formol concentration of 1.592 mg/m^3 in air, that means an obvious fluorescence response towards formol in air and makes $Eu_{0.059}Tb_{0.051}Gd_{0.89}$-DPON PVA film a promising fluorescence platform in practical application.

Polluting Ions Recognition Process

The as-prepared **$Eu_{0.059}Tb_{0.051}Gd_{0.89}$-DPON** (1 mg) was dispersed into distilled water (10 mL) to form an aqueous suspension and then various solutions of ions (1 mM) were added into this suspension. During the sensing measurements, the authors adopted the same excitation wavelength at 340 nm. Then, the suspension which contained **$Eu_{0.059}Tb_{0.051}Gd_{0.89}$-DPON** and additional ions were vibrated and mixed to form homogeneous solutions for luminescent measurements.

Cations detection in aqueous solution

In this work, 19 kinds of cations (Na^+, K^+, NH_4^+, Ag^+, Cu^+, Cu^{2+}, Ca^{2+}, Mg^{2+}, Zn^{2+}, Ba^{2+}, Co^{2+}, Cd^{2+}, Hg^{2+}, Mn^{2+}, Ni^{2+}, Fe^{2+}, Sn^{2+}, Fe^{3+}, Sn^{4+}) were chosen for

detection and their emission spectra excited under 340 nm are recorded in Fig. S19a. We can see that various cations (1 mM) have different degrees of quenching effect on the luminescence of $Eu_{0.059}Tb_{0.051}Gd_{0.89}$-DPON. The intensity of all three emission centers of ligand, Tb^{3+} and Eu^{3+} gradually decrease from Hg^{2+} to Fe^{3+} in Fig. S20a. Compared with the free $Eu_{0.059}Tb_{0.051}Gd_{0.89}$-DPON in water, four cations (Hg^{2+}, Cd^{2+}, Na^{+} and Ca^{2+}) exhibited weak effect on the luminescence of $Eu_{0.059}Tb_{0.051}Gd_{0.89}$-DPON, while NH_4^{+}, K^{+}, Ag^{+}, Co^{2+}, Mg^{2+}, Ba^{2+}, Zn^{2+} and Mn^{2+} slightly quenched the fluorescence, and the quenching capability of Ni^{2+}, Cu^{2+}, Sn^{2+}, Fe^{2+}, Cu^{+} and Sn^{4+} is significantly enhanced. When treated with Fe^{3+}, the emission bonds of both Ln^{3+} and ligand disappeared completely.

FT-IR spectra analysis

The FT-IR spectra are shown in Figures S4. The FT-IR spectra of all Ln-MOFs are similar, the hydroxyl group stretching vibration for the coordinated water molecules and free water molecules appear at 3500 cm^{-1}. The strong vibrations appearing at around 1540 cm^{-1} correspond to the asymmetric stretching vibration of the carboxylate group, while the strong vibrations appearing at around 1380 cm^{-1} correspond to the symmetric stretching vibration of the carboxylate group. The ($\nu_{as}(COO^{-}) - \nu_{s}(COO^{-})$) values of all Ln-MOFs are less than 200 cm^{-1}, indicating the chelating coordinate mode of carboxylate group in these Ln-MOFs. These are in good agreement with the results of single-crystal X-ray diffraction analysis.

TG analysis

As the TG curves shown in Figure S5, the weight lose before 170 °C is about 3.6%, which is attributed to the loss of free H_2O molecule in the structure. The weight

lose (7.1%) from 170 °C to 190 °C is attributed to the two H_2O molecules that coordinated with Ln^{3+}. Finally, the framework of Ln-MOFs begin to collapse at about 450 °C, proving the high stability of the Ln-MOFs. These weight lose are in good agreement with the results of single-crystal X-ray diffraction analysis.

PXRD analysis

As shown in Figure S6(a), the PXRD patterns of **1-Nd** ~ **6-Dy** and **$Eu_{0.059}Tb_{0.051}Gd_{0.89}$-DPON** are consistent with each other and match well with the simulation one. That means all Ln-MOFs are isomorphous. When the **$Eu_{0.059}Tb_{0.051}Gd_{0.89}$-DPON** is treated with Fe^{3+}, VO_4^{3-}, and formol, the framework integrity is confirmed by PXRD patterns in Figure S6(b). As for S^{2-}, the diffraction peak of **$Eu_{0.059}Tb_{0.051}Gd_{0.89}$-DPON** disappears and the crystallinity decreases which mean the framework collapse of **$Eu_{0.059}Tb_{0.051}Gd_{0.89}$-DPON** induced by S^{2-}.

Section 2. Structural Information.

Table S1 Crystallographic data and structural refinements for coordination polymers **1-Nd** ~ **6-Dy**.

	1-Nd	**2-Sm**	**3-Eu**	**4-Gd**	**5-Tb**	**6-Dy**
Empirical formula	$C_{14}H_{12}NdNO_{10}$	$C_{14}H_{12}SmNO_{10}$	$C_{14}H_{12}EuNO_{10}$	$C_{14}H_{12}GdNO_{10}$	$C_{14}H_{12}TbNO_{10}$	$C_{14}H_{12}DyNO_{10}$
Formula weight	498.49	504.6	506.21	511.5	513.17	516.75
Crystal system	Triclinic	Triclinic	Triclinic	Triclinic	Triclinic	Triclinic
Space group	*P***Error!**	*P***Error!**	*P***Error!**	*P***Error!**	*P***Error!**	*P***Error!**
a/Å	6.043(3)	6.006(3)	6.000(1)	5.979 (1)	5.962(2)	5.955 (1)
b/Å	11.817(6)	11.758(7)	11.778(2)	11.758(2)	11.757(4)	11.780(2)
c/Å	12.667(7)	12.603(7)	12.584(2)	12.574(2)	12.566(4)	12.542(2)
α (°)	110.247(5)	110.141(6)	110.091(1)	110.206(2)	110.209(4)	110.040(2)
β (°)	94.315(6)	94.201(7)	94.335(1)	94.086(2)	94.073(4)	94.431(2)
γ (°)	103.043(5)	102.980(6)	103.181(1)	103.083(2)	103.086(3)	103.214(2)
Volume/Å^3	815.0(7)	803.1(8)	801.5(2)	797.2(2)	794.3(4)	793.0(2)
Z	2	2	2	2	2	2
D_{calcd}/Mg·m^{-3}	2.031	2.087	2.098	2.131	2.146	2.164
μ/mm^{-1}	3.242	3.714	3.971	4.218	4.510	4.770
F(000)	486	490	492	494	496	498
θ range (°)	1.738 – 24.999	1.745 – 25.000	1.748 – 24.999	3.038 – 24.999	1.750 – 24.995	1.754 – 24.993
Limiting indices	-7≤h<≤7 –14≤*k*≤14 –15≤*l*≤15	-7≤h<≤6 –13≤*k*≤13 –14≤*l*≤14	-7≤h<≤7 –13≤*k*≤13 –14≤*l*≤14	-6≤h≤7 –13≤*k*≤13 –14≤*l*≤14	-7≤h≤7 –13≤*k*≤13 –14≤*l*≤12	-7≤h≤7 –13≤*k*≤13 –11≤*l*≤14
GOF on F^2	1.167	1.295	0.89	0.884	1.269	0.831
Final indices [$I > 2\sigma(I)$]	R R_1 [a]	0.0342	0.0297	0.0282	0.0302	0.0253	0.0277
	wR_2 [b]	0.0961	0.0820	0.0820	0.0760	0.0676	0.0800
R indices (all data)	R_1	0.0376	0.0358	0.0350	0.0371	0.0310	0.0363
	wR_2	0.1059	0.1088	0.1042	0.0787	0.0888	0.0994
CCDC		1873002	1873003	1873004	1873005	1873006	1873007

[a] $R_1 = \sum||F_o| - |F_c||/\sum|F_o|$. [b] $wR_2 = \{\sum[w\,(F_o^2 - F_c^2)^2]/\sum[\,w\,(F_o^2)^2]\}^{1/2}$

Table S2 Selected bond lengths (Å) and bond angles (°) for **1-Nd.**

Bond	Bond Lengths (Å)	Bond	Bond Lengths (Å)	Bond	Bond Lengths (Å)
Nd-O(1W)	2.412(4)	Nd-O(6)	2.475(4)	Nd-O(7)	2.528(5)
Nd-O(4)	2.439(4)	Nd-O(5)	2.500(4)	Nd-O(2)	2.551(5)
Nd-O(2W)	2.469(5)	Nd-O(3)	2.501(5)	Nd-O(4)	2.685(4)
Bond	Bond Angles (°)	Bond	Bond Angles (°)	Bond	Bond Angles (°)
O(1W)-Nd-O(4)	79.34(15)	O(2W)-Nd-O(3)	91.95(19)	O(6)-Nd-O(2)	127.36(16)
O(1W)-Nd-O(2W)	75.41(18)	O(6)-Nd-O(3)	79.71(16)	O(5)-Nd-O(2)	72.47(16)
O(4)-Nd-O(2W)	85.31(18)	O(5)-Nd-O(3)	79.76(16)	O(3)-Nd-O(2)	51.73(14)
O(1W)-Nd-O(6)	148.55(16)	O(1W)-Nd-O(7)	145.80(17)	O(7)-Nd-O(2)	117.39(17)
O(4)-Nd-O(6)	80.73(15)	O(4)-Nd-O(7)	80.70(17)	O(1W)-Nd-O(4)	74.09(15)
O(2W)-Nd-O(6)	126.75(16)	O(2W)-Nd-O(7)	75.53(17)	O(4)-Nd-O(4)	65.21(15)
O(1W)-Nd-O(5)	85.64(16)	O(6)-Nd-O(7)	51.63(14)	O(2W)-Nd-O(4)	140.71(16)
O(4)-Nd-O(5)	114.86(14)	O(5)-Nd-O(7)	128.12(16)	O(6)-Nd-O(4)	75.54(13)
O(2W)-Nd-O(5)	149.43(18)	O(3)-Nd-O(7)	72.87(18)	O(5)-Nd-O(4)	49.72(13)
O(6)-Nd-O(5)	80.98(15)	O(1W)-Nd-O(2)	73.98(15)	O(3)-Nd-O(4)	126.10(15)
O(1W)-Nd-O(3)	125.69(16)	O(4)-Nd-O(2)	151.77(15)	O(7)-Nd-O(4)	121.05(15)
O(4)-Nd-O(3)	153.25(15)	O(2W)-Nd-O(2)	79.28(19)	O(2)-Nd-O(4)	114.70(14)

Table S3 Selected bond lengths (Å) and bond angles (°) for **2-Sm.**

Bond	Bond Lengths (Å)	Bond	Bond Lengths (Å)	Bond	Bond Lengths (Å)
Sm(1)-O(2W)	2.382(5)	Sm(1)-O(5)	2.440(5)	Sm(1)-O(4)	2.509(6)
Sm(1)-O(6)	2.394(4)	Sm(1)-O(7)	2.467(5)	Sm(1)-O(2)	2.529(5)
Sm(1)-O(1W)	2.431(5)	Sm(1)-O(3)	2.476(5)	Sm(1)-O(6)	2.687(5)
Bond	Bond Angles (°)	Bond	Bond Angles (°)	Bond	Bond Angles (°)
O(2W)-Sm(1)-O(6)	79.05(17)	O(1W)-Sm(1)-O(3)	91.9(2)	O(5)-Sm(1)-O(2)	127.70(16)
O(2W)-Sm(1)-O(1W)	75.8(2)	O(5)-Sm(1)-O(3)	79.49(17)	O(7)-Sm(1)-O(2)	72.43(17)
O(6)-Sm(1)-O(1W)	85.29(19)	O(7)-Sm(1)-O(3)	79.88(17)	O(3)-Sm(1)-O(2)	52.26(16)
O(2W)-Sm(1)-O(5)	148.00(17)	O(2W)-Sm(1)-O(4)	145.91(18)	O(4)-Sm(1)-O(2)	117.29(18)
O(6)-Sm(1)-O(5)	80.99(17)	O(6)-Sm(1)-O(4)	80.88(18)	O(2W)-Sm(1)-O(6)	73.61(16)
O(1W)-Sm(1)-O(5)	127.05(19)	O(1W)-Sm(1)-O(4)	75.32(19)	O(6)-Sm(1)-O(6)	64.98(16)
O(2W)-Sm(1)-O(7)	84.84(18)	O(5)-Sm(1)-O(4)	52.13(16)	O(1W)-Sm(1)-O(6)	140.56(18)
O(6)-Sm(1)-O(7)	115.05(15)	O(7)-Sm(1)-O(4)	128.82(18)	O(5)-Sm(1)-O(6)	75.35(15)
O(1W)-Sm(1)-O(7)	148.8(2)	O(3)-Sm(1)-O(4)	72.6(2)	O(7)-Sm(1)-O(6)	50.11(14)
O(5)-Sm(1)-O(7)	81.28(17)	O(2W)-Sm(1)-O(2)	73.86(16)	O(3)-Sm(1)-O(6)	126.31(16)
O(2W)-Sm(1)-O(3)	126.12(17)	O(6)-Sm(1)-O(2)	151.17(17)	O(4)-Sm(1)-O(6)	121.18(17)
O(6)-Sm(1)-O(3)	153.17(18)	O(1W)-Sm(1)-O(2)	78.8(2)	O(2)-Sm(1)-O(6)	115.08(16)

Table S4 Selected bond lengths (Å) and bond angles (°) for **3-Eu.**

Bond	Bond Lengths (Å)	Bond	Bond Lengths (Å)	Bond	Bond Lengths (Å)
Eu(1)-O(1W)	2.373(4)	Eu(1)-O(6)	2.435(4)	Eu(1)-O(7)	2.496(5)
Eu(1)-O(5)	2.384(4)	Eu(1)-O(4)	2.451(4)	Eu(1)-O(2)	2.515(5)
Eu(1)-O(2W)	2.417(5)	Eu(1)-O(3)	2.460(4)	Eu(1)-O(5)	2.684(4)
Bond	Bond Angles (°)	Bond	Bond Angles (°)	Bond	Bond Angles (°)
O(1W)-Eu(1)-O(5)	79.14(15)	O(2W)-Eu(1)-O(3)	91.9(2)	O(6) -Eu(1)-O(2)	127.70(15)

O(1W)-Eu(1)-O(2W)	76.29(18)	O(6) -Eu(1)-O(3)	79.41(15)	O(4)-Eu(1)-O(2)	72.63(16)
O(5)-Eu(1)-O(2W)	85.12(18)	O(4)-Eu(1)-O(3)	80.16(16)	O(3)-Eu(1)-O(2)	52.55(14)
O(1W)-Eu(1)-O(6)	147.69(16)	O(1W)-Eu(1)-O(7)	145.96(17)	O(7) -Eu(1)-O(2)	117.67(17)
O(5)-Eu(1)-O(6)	80.90(15)	O(5)-Eu(1)-O(7)	80.55(16)	O(1W)-Eu(1)-O(5)	73.45(15)
O(2W)-Eu(1)-O(6)	126.87(17)	O(2W)-Eu(1)-O(7)	75.01(17)	O(5)-Eu(1)-O(5)	64.72(16)
O(1W)-Eu(1)-O(4)	84.87(16)	O(6)-Eu(1)-O(7)	52.25(15)	O(2W)-Eu(1)-O(5)	140.44(17)
O(5)-Eu(1)-O(4)	114.82(14)	O(4)-Eu(1)-O(7)	128.65(16)	O(6)-Eu(1)-O(5)	75.13(13)
O(2W)-Eu(1)-O(4)	149.56(19)	O(3)-Eu(1)-O(7)	72.63(17)	O(4)-Eu(1)-O(5)	50.16(13)
O(6)-Eu(1)-O(4)	80.80(15)	O(1W)-Eu(1)-O(2)	73.82(15)	O(3)-Eu(1)-O(5)	126.64(16)
O(1W)-Eu(1)-O(3)	126.37(15)	O(5)-Eu(1)-O(2)	151.24(15)	O(7)-Eu(1)-O(5)	120.82(15)
O(5)-Eu(1)-O(3)	152.85(16)	O(2W)-Eu(1)-O(2)	79.2(2)	O(2)-Eu(1)-O(5)	115.18(15)

Table S5 Selected bond lengths (Å) and bond angles (°) for **4-Gd.**

Bond	Bond Lengths (Å)	Bond	Bond Lengths (Å)	Bond	Bond Lengths (Å)
Gd(1)-O(1W)	2.358(4)	Gd(1)-O(5)	2.421(4)	Gd(1)-O(4)	2.486(4)
Gd(1)-O(6)	2.366(4)	Gd(1)-O(7)	2.434(4)	Gd(1)-O(2)	2.501(4)
Gd(1)-O(2W)	2.403(4)	Gd(1)-O(3)	2.447(4)	Gd(1)-O(6)	2.694(4)
Bond	Bond Angles (°)	Bond	Bond Angles (°)	Bond	Bond Angles (°)
O(1W)-Gd(1)-O(6)	78.64(14)	O(2W)-Gd(1)-O(3)	91.65(16)	O(5)-Gd(1)-O(2)	127.98(13)
O(1W)-Gd(1)-O(2W)	76.24(15)	O(5)-Gd(1)-O(3)	79.31(14)	O(7)-Gd(1)-O(2)	72.70(14)
O(6)-Gd(1)-O(2W)	85.50(16)	O(7)-Gd(1)-O(3)	80.20(13)	O(3)-Gd(1)-O(2)	52.76(13)
O(1W)-Gd(1)-O(5)	147.50(14)	O(1W)-Gd(1)-O(4)	145.63(14)	O(4)-Gd(1)-O(2)	117.53(15)
O(6)-Gd(1)-O(5)	81.13(13)	O(6)-Gd(1)-O(4)	80.70(14)	O(1W)-Gd(1)-O(6)	73.41(13)
O(2W)-Gd(1)-O(5)	127.18(14)	O(2W)-Gd(1)-O(4)	75.01(15)	O(6)-Gd(1)-O(6)	64.72(13)
O(1W)-Gd(1)-O(7)	84.58(14)	O(5)-Gd(1)-O(4)	52.50(13)	O(2W)-Gd(1)-O(6)	140.78(14)
O(6)-Gd(1)-O(7)	114.90(12)	O(7)-Gd(1)-O(4)	129.27(14)	O(5)-Gd(1)-O(6)	75.02(12)
O(2W)-Gd(1)-O(7)	148.74(17)	O(3)-Gd(1)-O(4)	72.67(15)	O(7)-Gd(1)-O(6)	50.20(11)
O(5)-Gd(1)-O(7)	81.19(13)	O(1W)-Gd(1)-O(2)	73.94(13)	O(3)-Gd(1)-O(6)	126.51(13)
O(1W)-Gd(1)-O(3)	126.70(14)	O(6)-Gd(1)-O(2)	150.75(14)	O(4)-Gd(1)-O(6)	120.91(14)
O(6)-Gd(1)-O(3)	153.01(14)	O(2W)-Gd(1)-O(2)	78.34(17)	O(2)-Gd(1)-O(6)	115.46(13)

Table S6 Selected bond lengths (Å) and bond angles (°) for **5-Tb.**

Bond	Bond Lengths (Å)	Bond	Bond Lengths (Å)	Bond	Bond Lengths (Å)
Tb(1)-O(1W)	2.344(4)	Tb(1)-O(5)	2.406(4)	Tb(1)-O(4)	2.474(5)
Tb(1)-O(6)	2.353(4)	Tb(1)-O(7)	2.417(4)	Tb(1)-O(2)	2.488(5)
Tb(1)-O(2W)	2.388(5)	Tb(1)-O(3)	2.432(4)	Tb(1)-O(6)	2.711(4)
Bond	Bond Angles (°)	Bond	Bond Angles (°)	Bond	Bond Angles (°)
O(1W)-Tb(1)-O(6)	78.68(15)	O(2W)-Tb(1)-O(3)	92.15(18)	O(5)-Tb(1)-O(2)	128.21(14)
O(1W)-Tb(1)-O(2W)	76.56(17)	O(5)-Tb(1)-O(3)	79.48(15)	O(7)-Tb(1)-O(2)	72.99(16)
O(6)-Tb(1)-O(2W)	85.04(17)	O(7)-Tb(1)-O(3)	80.42(15)	O(3)-Tb(1)-O(2)	52.92(14)
O(1W)-Tb(1)-O(5)	147.02(15)	O(1W)-Tb(1)-O(4)	145.69(16)	O(4)-Tb(1)-O(2)	117.43(16)
O(6)-Tb(1)-O(5)	80.95(15)	O(6)-Tb(1)-O(4)	80.86(16)	O(1W)-Tb(1)-O(6)	73.35(14)
O(2W)-Tb(1)-O(5)	127.09(16)	O(2W)-Tb(1)-O(4)	74.47(17)	O(6)-Tb(1)-O(6)	64.42(15)
O(1W)-Tb(1)-O(7)	84.30(15)	O(5)-Tb(1)-O(4)	53.05(14)	O(2W)-Tb(1)-O(6)	140.43(16)
O(6)-Tb(1)-O(7)	114.46(14)	O(7)-Tb(1)-O(4)	129.48(15)	O(5)-Tb(1)-O(6)	74.53(13)
O(2W)-Tb(1)-O(7)	149.50(19)	O(3)-Tb(1)-O(4)	72.59(17)	O(7)-Tb(1)-O(6)	50.06(13)
O(5)-Tb(1)-O(7)	80.88(14)	O(1W)-Tb(1)-O(2)	73.82(14)	O(3)-Tb(1)-O(6)	126.52(15)
O(1W)-Tb(1)-O(3)	126.74(15)	O(6)-Tb(1)-O(2)	150.67(15)	O(4)-Tb(1)-O(6)	120.95(15)
O(6)-Tb(1)-O(3)	153.05(16)	O(2W)-Tb(1)-O(2)	78.93(19)	O(2)-Tb(1)-O(6)	115.65(14)

Table S7 Selected bond lengths (Å) and bond angles (°) for **6-Dy.**

Bond	Bond Lengths (Å)	Bond	Bond Lengths (Å)	Bond	Bond Lengths (Å)
Dy(1)-O(1W)	2.325(4)	Dy(1)-O(6)	2.392(4)	Dy(1)-O(7)	2.468(5)
Dy(1)-O(4)	2.336(4)	Dy(1)-O(5)	2.408(5)	Dy(1)-O(3)	2.481(5)
Dy(1)-O(2W)	2.379(5)	Dy(1)-O(2)	2.422(5)	Dy(1)-O(4)	2.723(5)
Bond	Bond Angles (°)	Bond	Bond Angles (°)	Bond	Bond Angles (°)
O(1W)-Dy(1)-O(4)	78.50(16)	O(2W)-Dy(1)-O(2)	91.9(2)	O(6)-Dy(1)-O(3)	128.40(16)
O(1W)-Dy(1)-O(2W)	76.27(19)	O(6)-Dy(1)-O(2	79.45(16)	O(5)-Dy(1)-O(3)	72.98(17)
O(4)-Dy(1)-O(2W)	85.7(2)	O(5)-Dy(1)-O(2)	80.56(17)	O(2)-Dy(1)-O(3)	53.36(15)
O(1W)-Dy(1)-O(6)	147.05(17)	O(1W)-Dy(1)-O(7)	145.26(18)	O(7)-Dy(1)-O(3)	117.94(18)
O(4)-Dy(1)-O(6)	80.81(16)	O(4)-Dy(1)-O(7)	80.89(17)	O(1W)-Dy(1)-O(4)	73.77(16)
O(2W)-Dy(1)-O(6)	127.35(18)	O(2W)-Dy(1)-O(7)	74.55(19)	O(4)-Dy(1)-O(4)	64.06(17)
O(1W)-Dy(1)-O(5)	84.78(17)	O(6)-Dy(1)-O(7)	53.18(16)	O(2W)-Dy(1)-O(4)	140.77(18)
O(4)-Dy(1)-O(5)	114.00(16)	O(5)-Dy(1)-O(7)	129.39(17)	O(6)-Dy(1)-O(4)	74.19(14)
O(2W)-Dy(1)-O(5)	149.5(2)	O(2)-Dy(1)-O(7)	72.60(18)	O(5)-Dy(1)-O(4)	49.97(14)
O(6)-Dy(1)-O(5)	80.56(16)	O(1W)-Dy(1)-O(3)	73.61(16)	O(2)-Dy(1)-O(4)	126.50(16)
O(1W)-Dy(1)-O(2)	126.96(16)	O(4)-Dy(1)-O(3)	150.54(17)	O(7)-Dy(1)-O(4)	120.67(17)
O(4)-Dy(1)-O(2)	153.04(17)	O(2W)-Dy(1)-O(3)	78.8(2)	O(3)-Dy(1)-O(4)	115.46(16)

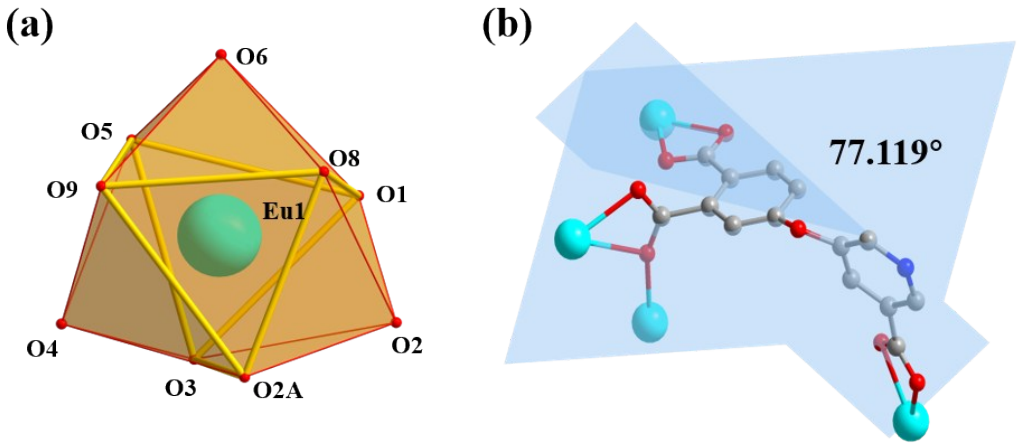

Figure S1. (a) Twisted tri-capped triangular prismatic geometry of Eu^{3+} in 3-Eu. (b) The dihedral angle between benzene ring and pyridine ring in ligand.

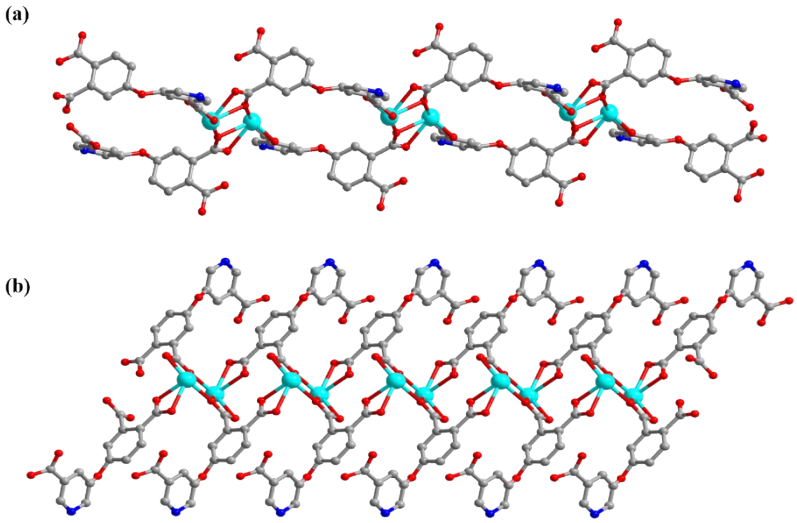

Figure S2. The one-dimensional chains structure along the a axis (a) and b axis (b).

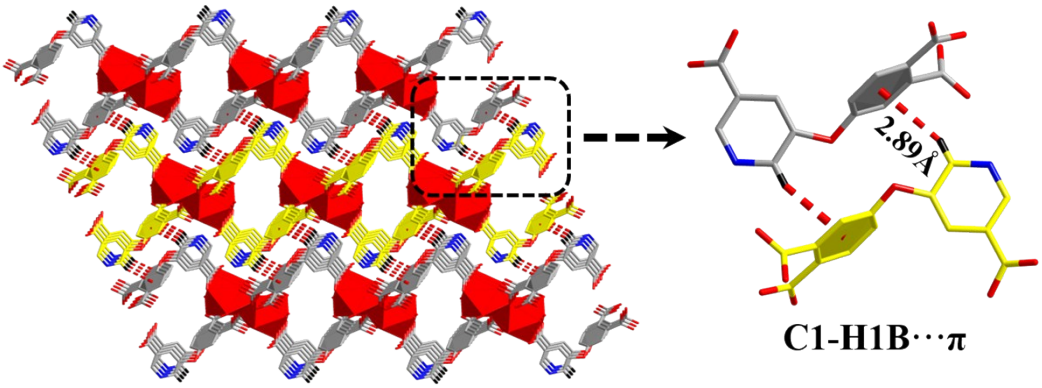

Figure S3. The 3D structure constructed by hydrogen bonding (C1-H1B···π).

Section 3. Crystal structure characterizations of Ln-MOFs.

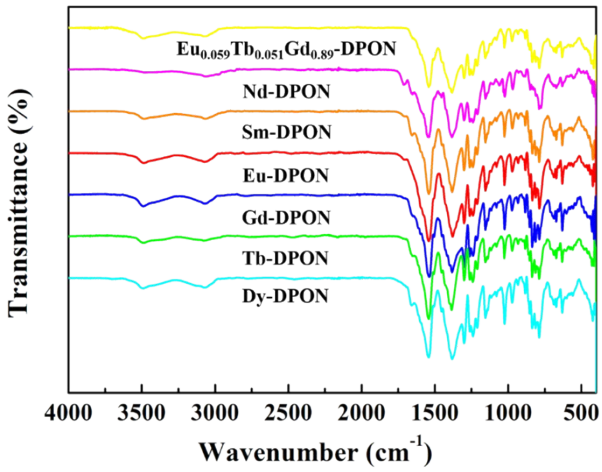

Figure S4. FT-IR spectra of **1-Nd** ~ **6-Dy** and **$Eu_{0.059}Tb_{0.051}Gd_{0.89}$-DPON**.

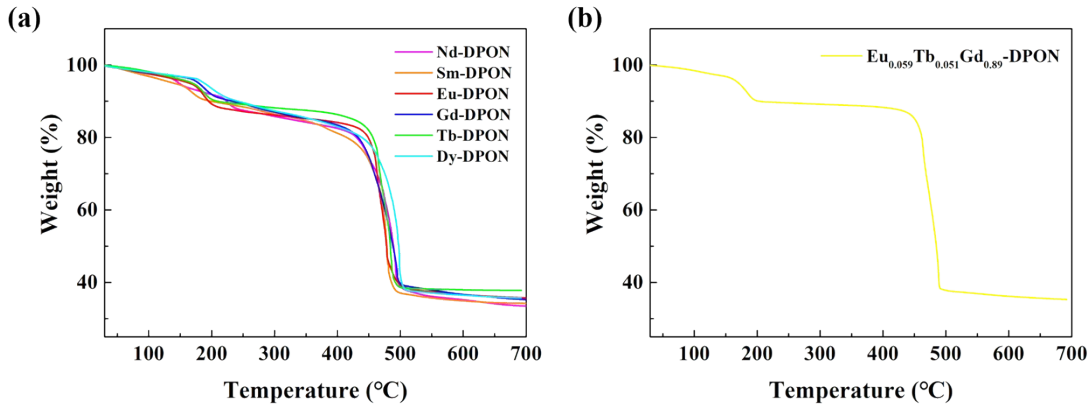

Figure S5. TG curves of (a) **1-Nd** ~ **6-Dy** and (b) **$Eu_{0.059}Tb_{0.051}Gd_{0.89}$-DPON**.

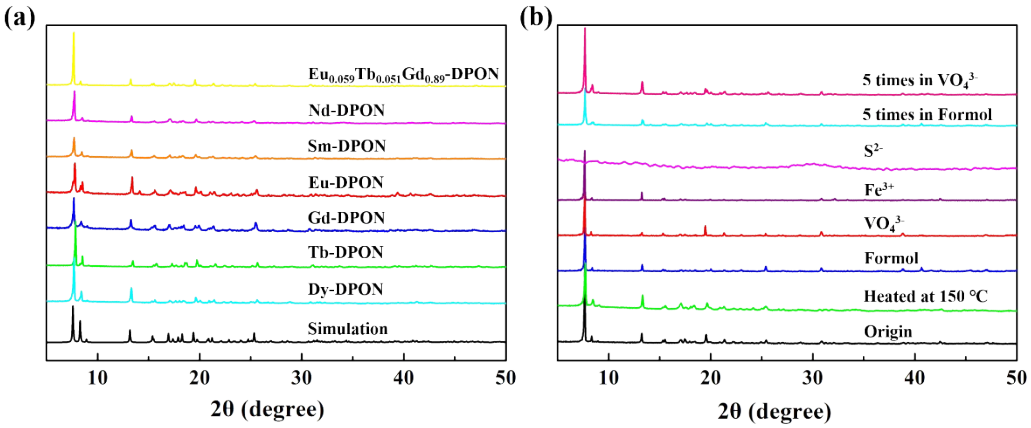

Figure S6. (a) PXRD patterns of **1-Nd** ~ **6-Dy** and **$Eu_{0.059}Tb_{0.051}Gd_{0.89}$-DPON**. (b) PXRD patterns of **$Eu_{0.059}Tb_{0.051}Gd_{0.89}$-DPON** heated at 150℃ or treated by various substances.

Table S8 The ICP-MS results of **$Eu_{0.059}Tb_{0.051}Gd_{0.89}$-DPON**

sample	Molar ratio of the reactant Eu/Tb/Gd salt	Eu/Tb/Gd mass ratio (ppm/ppm)	Eu/Tb/Gd molar ratio
$Eu_{0.059}Tb_{0.051}Gd_{0.89}$-DPON	5.9:5.1:89	1.128:1.011:17.488	5.94:5.09:88.97

Section 4. The Fluorescence performance of Ln-MOFs.

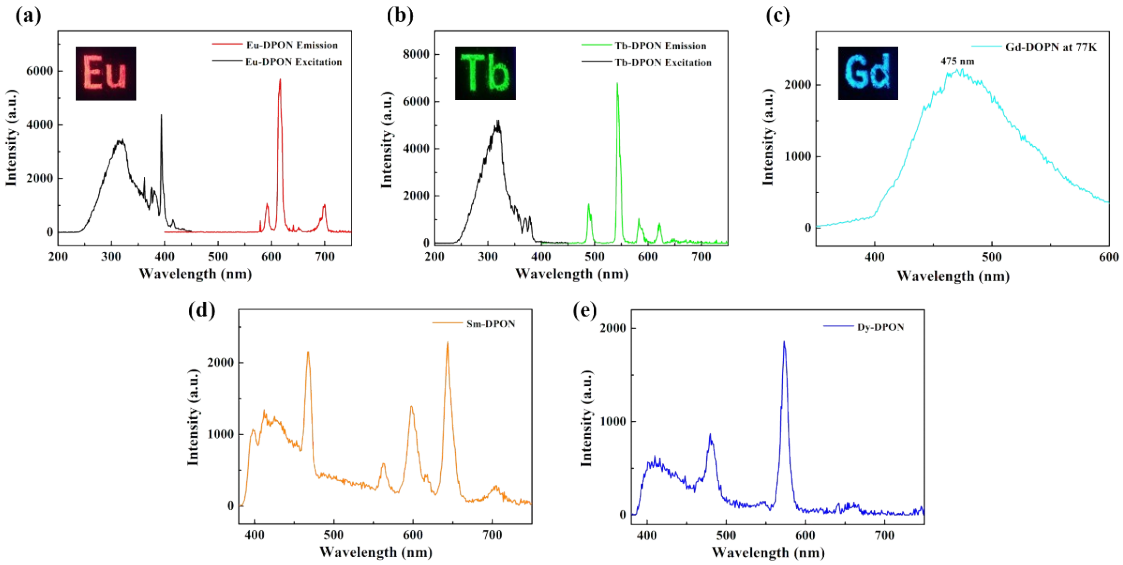

Figure S7. The excitation and emission spectra of (a) **3-Eu**, (b) **5-Tb**, (c) **4-Gd**, (d) **2-Sm** and (e) **6-Dy** excited at 321 nm.

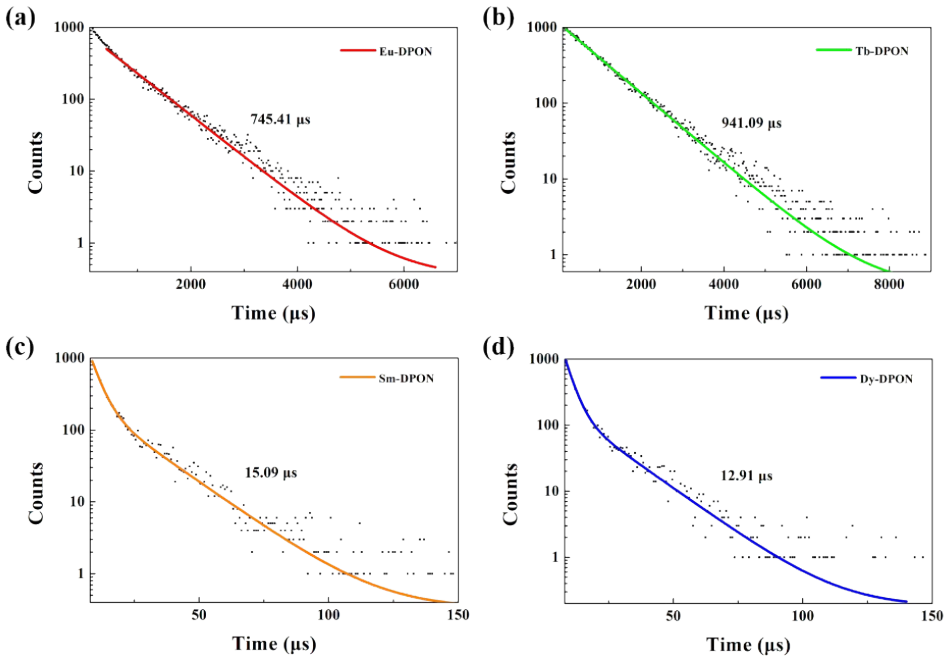

Figure S8. The fluorescence lifetime of (a) **3-Eu**, (b) **5-Tb**, (c) **2-Sm** and (d) **6-Dy** excited at 321 nm.

Table S9 Quantum yields (Φ) of pre and post heating Ln-MOFs.

Φ%	**3-Eu**	**5-Tb**	**$Eu_{0.059}Tb_{0.051}Gd_{0.89}$-DPON**
Original	10.5	41.8	15.2
Heated at 150 ℃ for 12 h	11.2	40.5	14.9

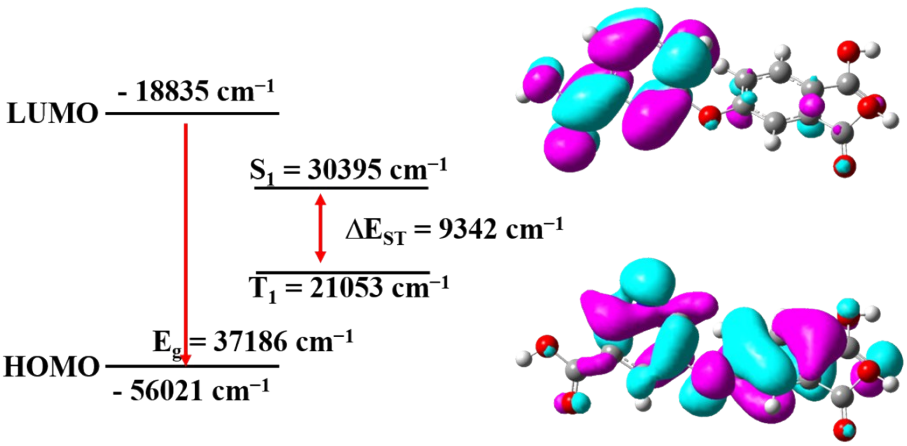

Figure S9. The calculated result of H_3DPON ligand through DFT calculations at the B3LYP/6-31 G* level.

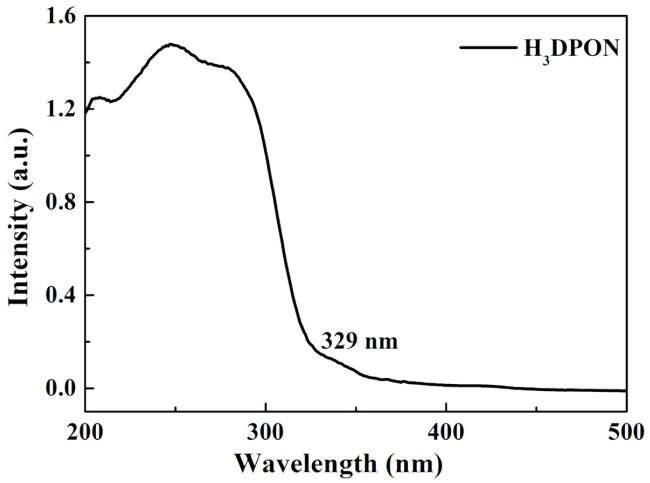

Figure S10. The UV-vis spectrum of H_3DPON ligand.

Section 5. Fluorescent Response Mechanism.

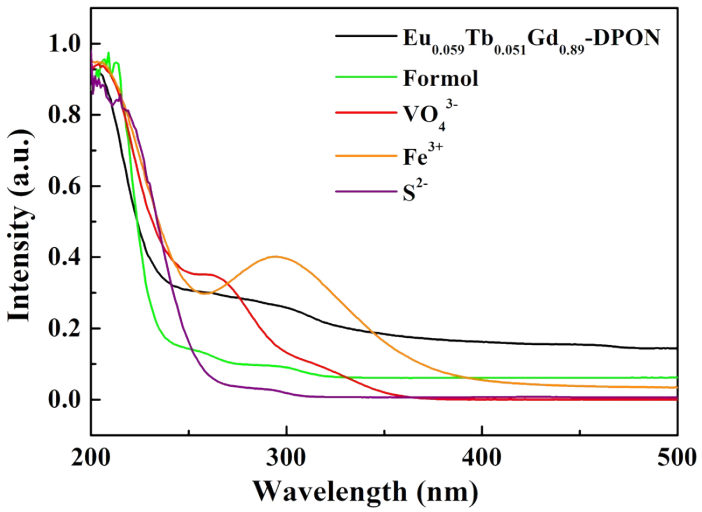

Figure S11. The UV-vis spectra of **$Eu_{0.059}Tb_{0.051}Gd_{0.89}$-DPON**, formol, VO_4^{3-}, Fe^{3+} and S^{2-} aqueous solution.

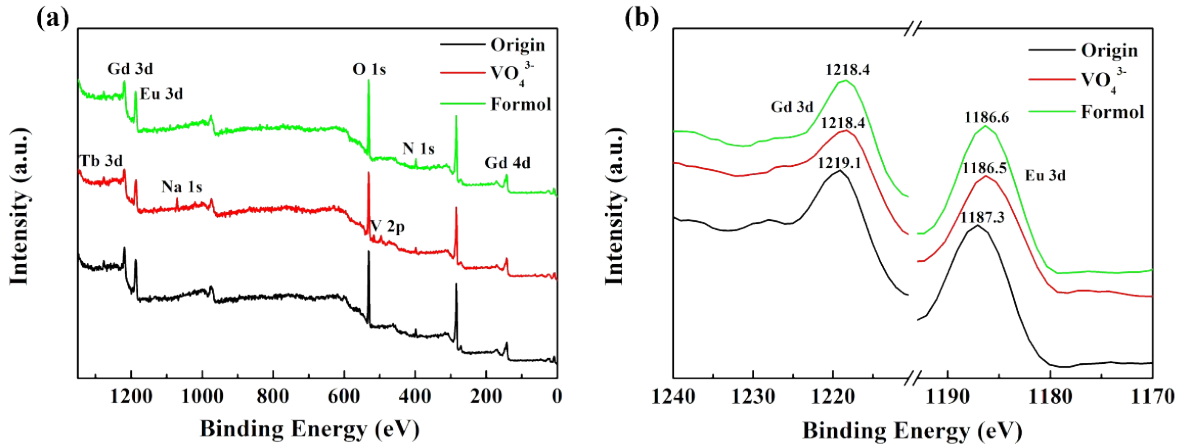

Figure S12. (a) XPS spectra and (b) Gd 3d and Eu 3d spectra of original **$Eu_{0.059}Tb_{0.051}Gd_{0.89}$-DPON** as well as it treated with formol or VO_4^{3-}.

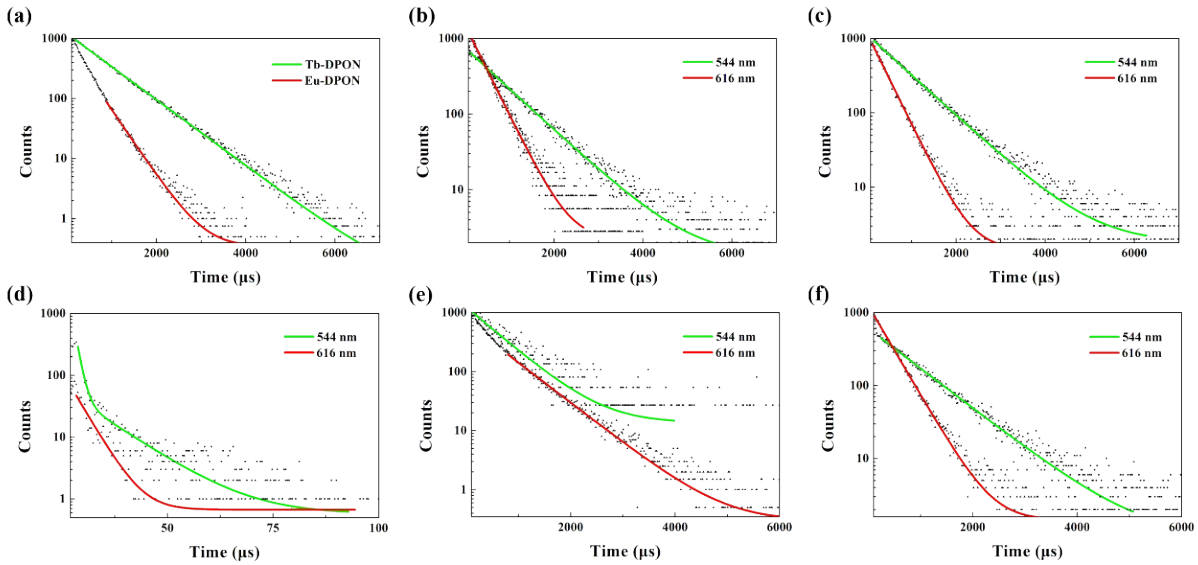

Figure S13. The fluorescence lifetimes of (a) **Eu-DPON** and **Tb-DPON**, (b) original **$Eu_{0.059}Tb_{0.051}Gd_{0.89}$-DPON**, (c) **$Eu_{0.059}Tb_{0.051}Gd_{0.89}$-DPON** in water, (d) **$Eu_{0.059}Tb_{0.051}Gd_{0.89}$-DPON** in Fe^{3+} aqueous solution, (e) **$Eu_{0.059}Tb_{0.051}Gd_{0.89}$-DPON** in VO_4^{3-} aqueous solution and (f) **$Eu_{0.059}Tb_{0.051}Gd_{0.89}$-DPON** in formol excited at 340 nm.

Table S10 The HOMO, LUMO and T_1 energy level of ligand, formol, acetaldehyde and acetone obtained through the DFT calculation at the B3LYP/6-31 G* level.

Molecules	HOMO (eV)	LUMO (eV)	T_1 (cm^{-1})
Ligand	-6.96	-2.34	21053
Formol	-7.37	-1.54	24109
Acetaldehyde	-7.00	-1.08	26132
Acetone	-6.68	-0.74	27470

Table S11 Fluorescence lifetimes at 544 nm and 616 nm of **Tb-DPON**, **Eu-DPON** and **$Eu_{0.059}Tb_{0.051}Gd_{0.89}$-DPON** in various conditions with excitation under 340 nm.

No.	Fluorescence lifetime at 544 nm (ms)	Fluorescence lifetime at 616 nm (ms)
Eu-DPON	--	0.39581
Tb-DPON	0.79073	--
$Eu_{0.059}Tb_{0.051}Gd_{0.89}$-DPON	0.80077	0.36240
$Eu_{0.059}Tb_{0.051}Gd_{0.89}$-DPON in H_2O	0.79703	0.35298
$Eu_{0.059}Tb_{0.051}Gd_{0.89}$-DPON in Fe^{3+}	0.00865	0.00372
$Eu_{0.059}Tb_{0.051}Gd_{0.89}$-DPON in VO_4^{3-}	0.57791	0.63841
$Eu_{0.059}Tb_{0.051}Gd_{0.89}$-DPON in formol	0.79266	0.35372

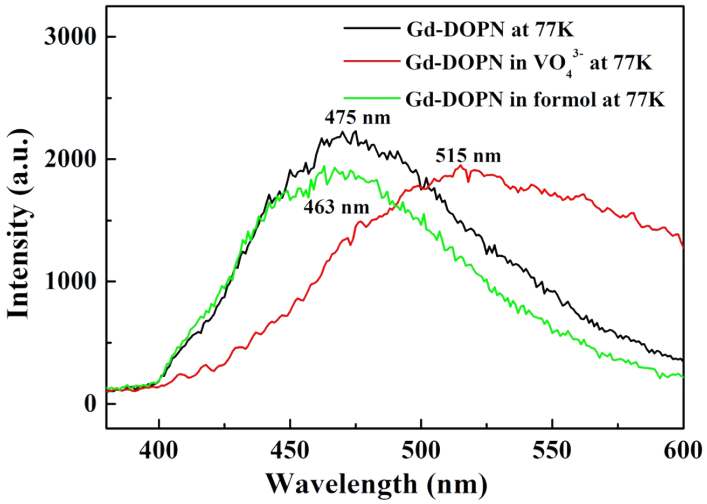

Figure S14. The emission spectra of original **$Gd_{0.89}$-DPON** as well as it treated with formol or VO_4^{3-} measured at 77K.

Section 6. The Detection for Formol.

Table S12 Standard deviation and limit of detection calculation for **$Eu_{0.059}Tb_{0.051}Gd_{0.89}$-DPON** toward formol.

No.	Luminescence Intensity (I_{544}) of $Eu_{0.059}Tb_{0.051}Gd_{0.89}$-DPON in H_2O	I_0/I-1
1	2944.48 a.u.	0
2	2942.44 a.u.	0.00069
3	2956.86 a.u.	-0.00419
4	2941.13 a.u.	0.00114
5	2948.83 a.u.	-0.00148
Standard Deviation (σ)	--	0.002154825
K_{SV}	--	0.33504 vol %$^{-1}$
Detection limit ($3\sigma/K_{SV}$)	--	0.0193 vol %

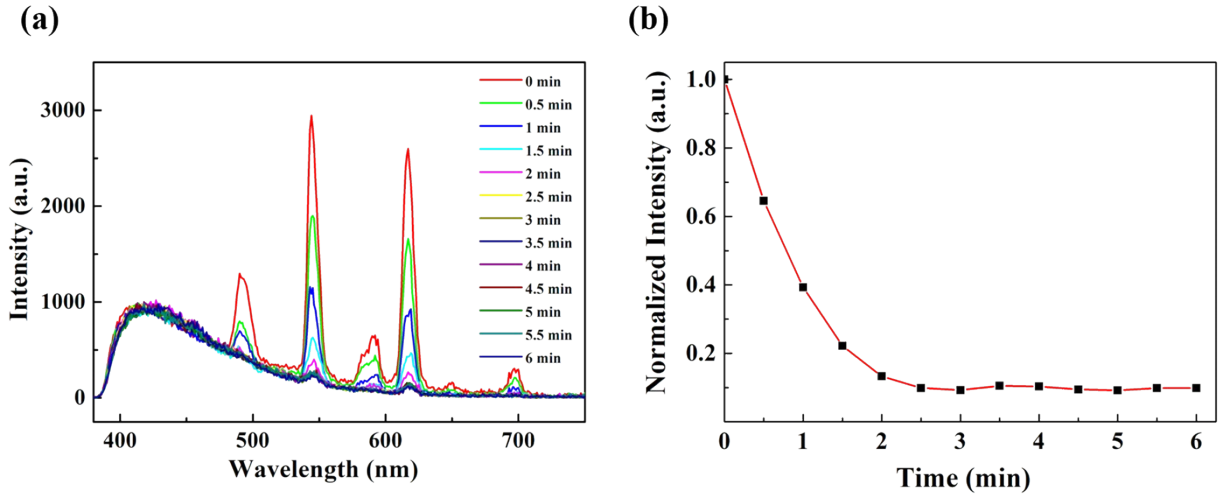

Figure S15. The fluorescence quench of **$Eu_{0.059}Tb_{0.051}Gd_{0.89}$-DPON** in 0-6 minutes after the addition of formol.

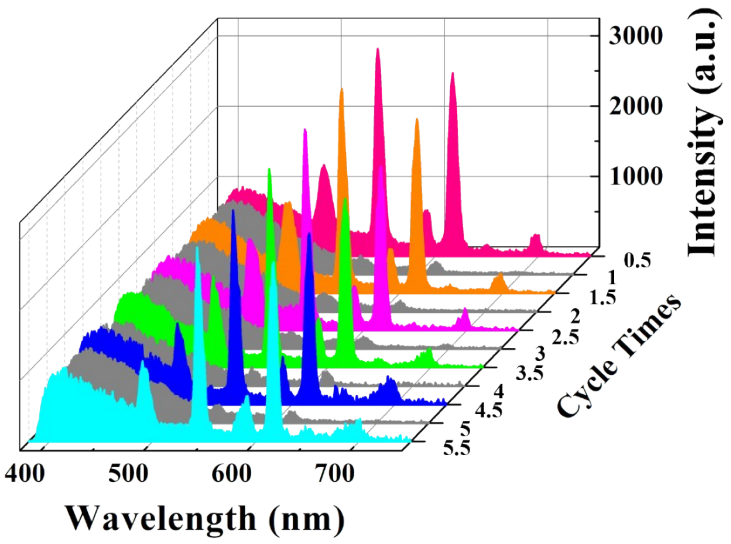

Figure S16. The emission spectra of **$Eu_{0.059}Tb_{0.051}Gd_{0.89}$-DPON** after five cycles in formol.

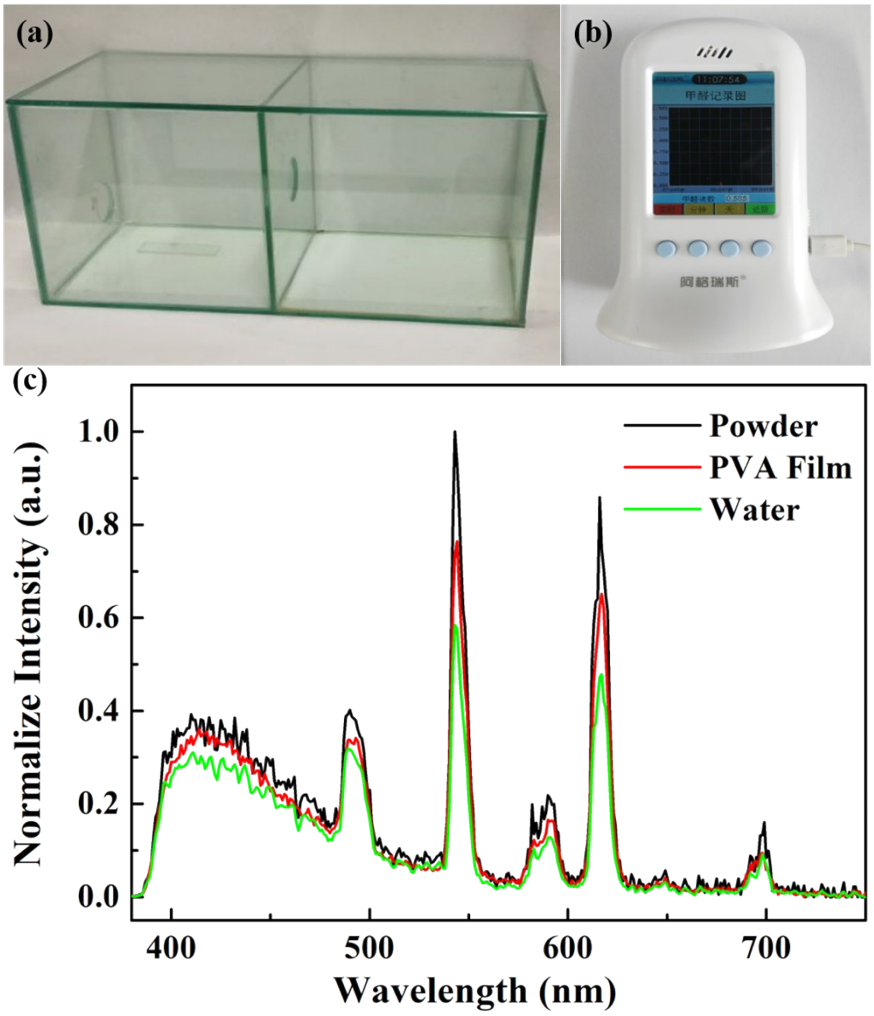

Figure S17. The photo of (a) device, (b) formol detector and (c)The emission spectra of **$Eu_{0.059}Tb_{0.051}Gd_{0.89}$-DPON** power, **$Eu_{0.059}Tb_{0.051}Gd_{0.89}$-DPON** PVA film and **$Eu_{0.059}Tb_{0.051}Gd_{0.89}$-DPON** in water.

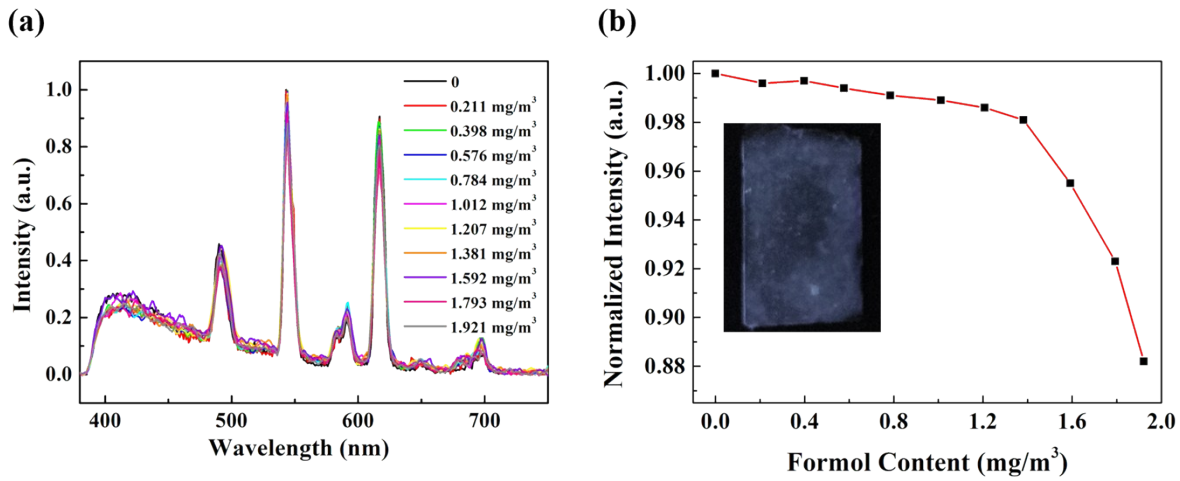

Figure S18. The fluorescence quench of **$Eu_{0.059}Tb_{0.051}Gd_{0.89}$-DPON** PVA film toward different concentrations of formol in air, insets show the corresponding photograph.

Section 7. 3D Decoded Map.

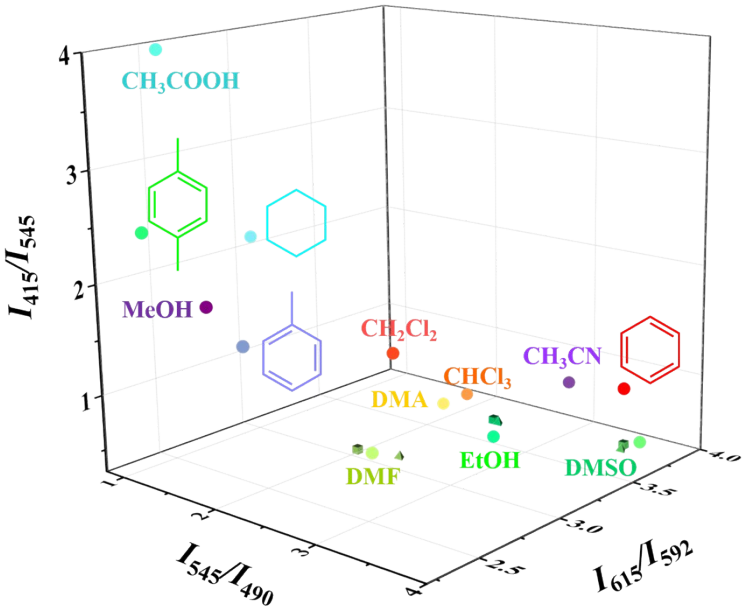

Figure S19. The 3D decoded map for various solvent molecules based on the ratios of I_{544}/I_{491}, I_{616}/I_{592} and I_{415}/I_{544}, the cube represent contents of DMF, DMSO or EtOH is 30 vol % and tetrahedron represent contents of DMF, DMSO or EtOH is 50 vol %.

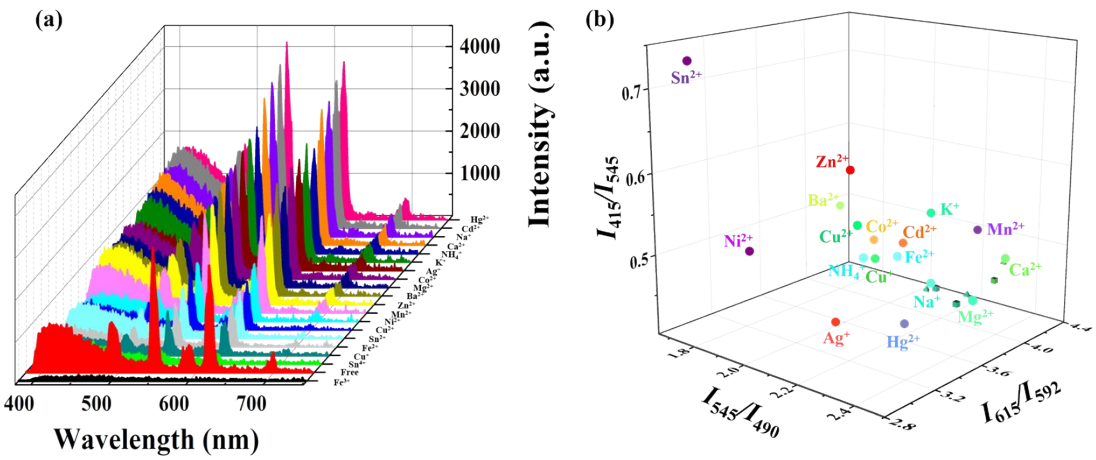

Figure S20. (a) Fluorescence response of **$Eu_{0.059}Tb_{0.051}Gd_{0.89}$-DPON** treated by different metal ions (1 mM aqueous solution for 30 min) excited at 340 nm. (b) The 3D decoded map for various metal ions based on the ratios of I_{544}/I_{491}, I_{616}/I_{592} and I_{415}/I_{544}, the cube represent concentrations of Na^+, Ca^{2+} or Mg^{2+} is 0.5 mM and tetrahedron represent contents of Na^+, Ca^{2+} or Mg^{2+} is 5 mM.

Section 8. The Detection for VO_4^{3-}.

Table S13 Standard deviation and limit of detection calculation for **$Eu_{0.059}Tb_{0.051}Gd_{0.89}$-DPON** toward VO_4^{3-}.

No.	Luminescence Intensity (I_{544}) of $Eu_{0.059}Tb_{0.051}Gd_{0.89}$-DPON in H_2O	Luminescence Intensity (I_{616}) of $Eu_{0.059}Tb_{0.051}Gd_{0.89}$-DPON in H_2O	I_{616}/I_{544}
1	2944.48 a.u.	2528.40 a.u.	0.858692
2	2942.44 a.u.	2523.37 a.u.	0.857577
3	2956.86 a.u.	2536.63 a.u.	0.857880
4	2941.13 a.u.	2525.19 a.u.	0.858578
5	2948.83 a.u.	2533.28 a.u.	0.859080
Standard Deviation (σ)	--	--	0.000640298
Slope (*S*)	--	--	4.55968 mM^{-1}
Detection limit (3σ/*S*)	--	--	0.42 μM

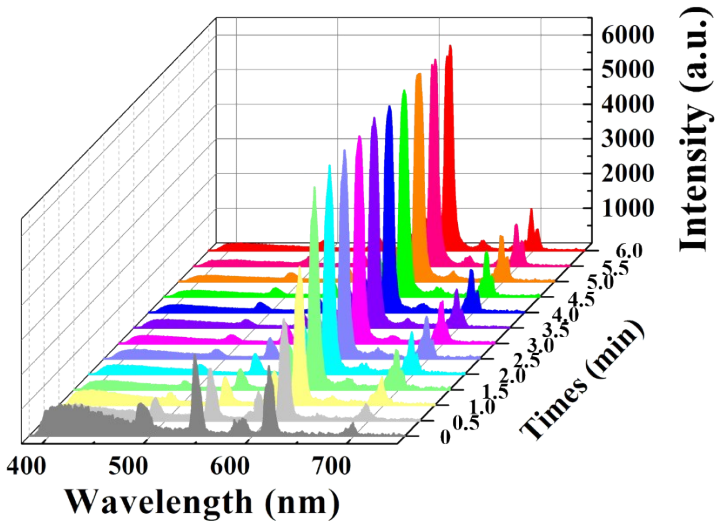

Figure S21. The emission spectra of **$Eu_{0.059}Tb_{0.051}Gd_{0.89}$-DPON** in 0-6 minutes after the addition of Na_3VO_4.

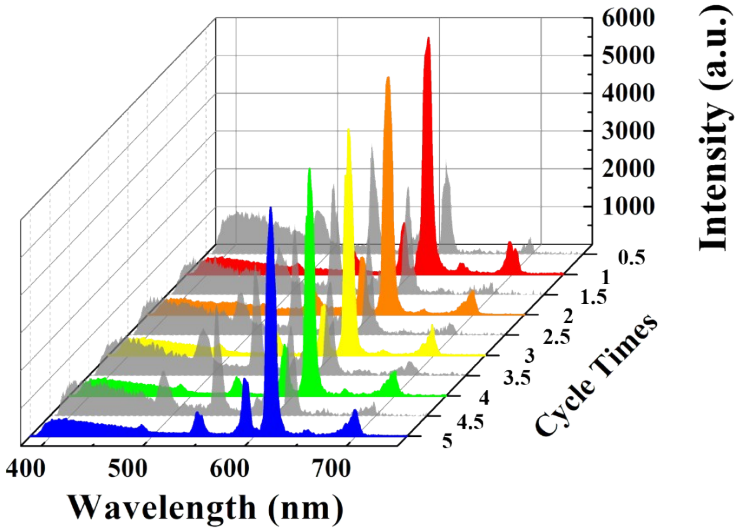

Figure S22. The emission spectra of **$Eu_{0.059}Tb_{0.051}Gd_{0.89}$-DPON** after five cycles in Na_3VO_4.

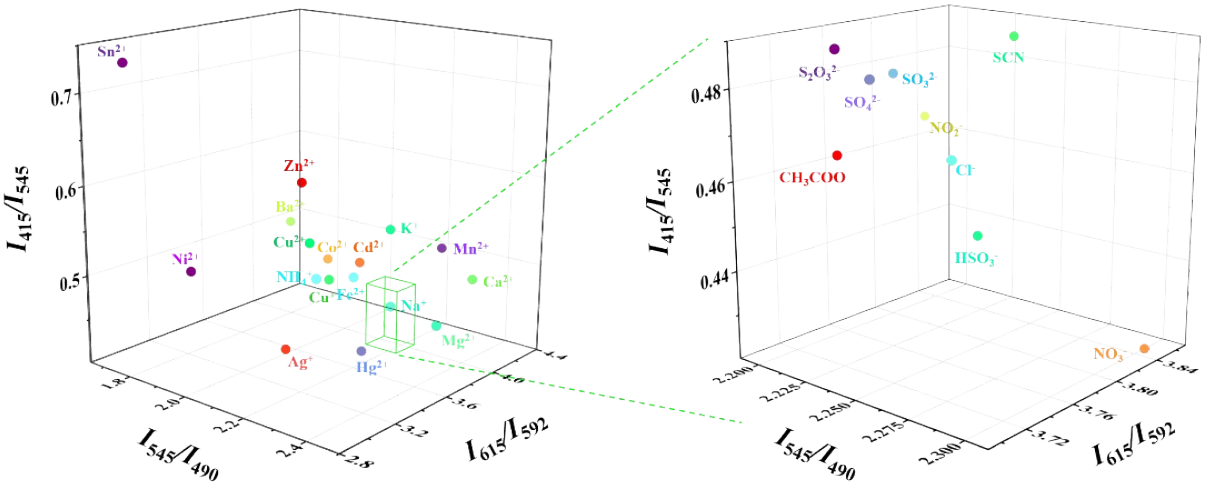

Figure S23. The 3-D decoded map for various anions.

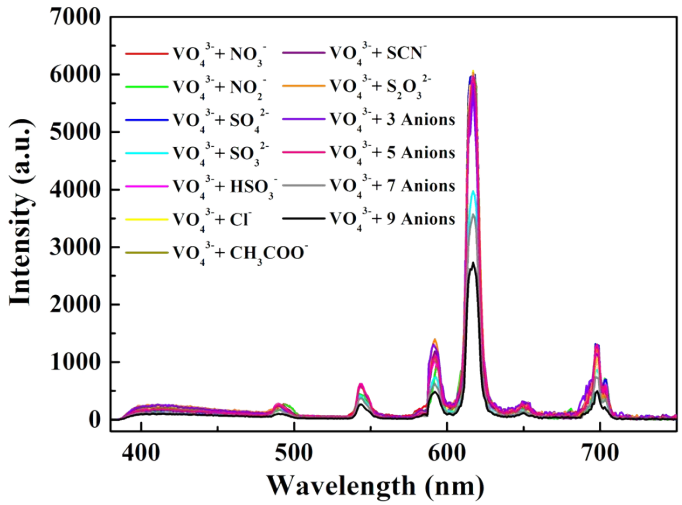

Figure S24. The emission spectra of **$Eu_{0.059}Tb_{0.051}Gd_{0.89}$-DPON** with one or more interfering anions.

Section 9. Boolean logic operation.

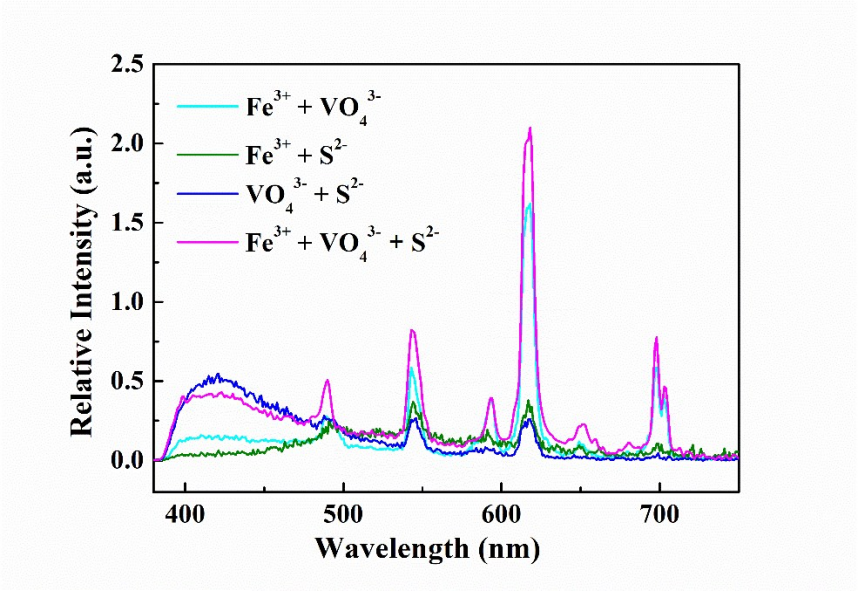

Figure S25. The emission spectra of **$Eu_{0.059}Tb_{0.051}Gd_{0.89}$-DPON** with double or three inputs.

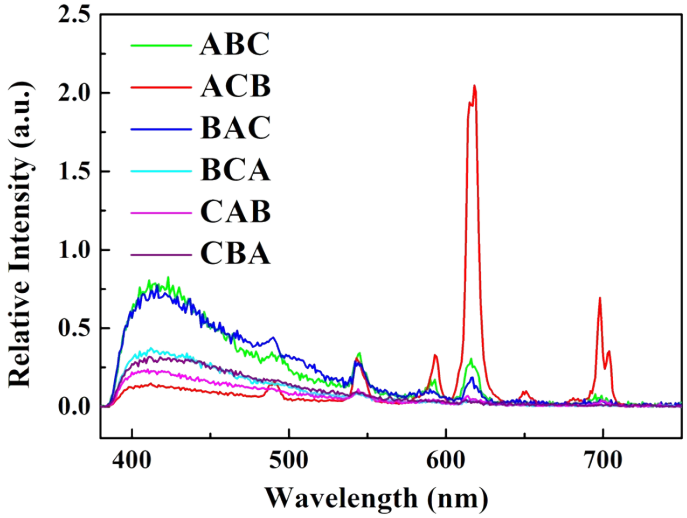

Figure S26. The emission spectra of **$Eu_{0.059}Tb_{0.051}Gd_{0.89}$-DPON** with different sequences of three inputs.